THE JOURNAL OF PHYSICAL CHEMISTRY C

Article

Cite This: J. Phys. Chem. C 2020, 124, 287−299

pubs.acs.org/JPCC

Volatile Etch Species Produced during Thermal Al_2O_3 Atomic Layer Etching

Joel W. Clancey, Andrew S. Cavanagh, James E. T. Smith, Sandeep Sharma, and Steven M. George*

Department of Chemistry, University of Colorado Boulder, Boulder, Colorado 80309, United States

ABSTRACT: The thermal atomic layer etching (ALE) of Al_2O_3 can be achieved using sequential fluorination and ligand-exchange reactions. Although previous investigations have characterized the etch rates and surface chemistry, no reports have identified the volatile etch products. This study explored the volatile etch species during thermal Al_2O_3 ALE at 300 °C using quadrupole mass spectrometry (QMS). HF was the fluorination reactant; $Al(CH_3)_3$ (trimethylaluminum (TMA)) and $AlCl(CH_3)_2$ (dimethylaluminum chloride, (DMAC)) were the metal precursors for ligand exchange. When TMA was used as the metal precursor after the fluorination of Al_2O_3 powder, the QMS measurements revealed that the main ion species were consistent with dimers of $AlF(CH_3)_2$ (dimethylaluminum fluoride (DMAF)) with itself (DMAF + DMAF) or with TMA (DMAF + TMA). These ion species were observed after loss of a methyl group as $Al_2F_2(CH_3)_3^+$ at m/z = 137 and $Al_2F(CH_3)_4^+$ at m/z = 133, respectively. In addition, an ion species consistent with a trimer was also observed as $Al_3F_3(CH_3)_5^+$ at m/z = 213. Very similar results were observed for TMA exposures on AlF_3 powder. Comparable results were also obtained using DMAC as the metal precursor for ligand exchange. In contrast, $SiCl_4$ and $TiCl_4$ are not successful metal precursors because they do not lead to thermal Al_2O_3 ALE at 300 °C. QMS measurements revealed no Al-containing etch species after $SiCl_4$ and $TiCl_4$ exposures on AlF_3 powder. However, $SiF_xCl_y^+$ and $TiF_xCl_y^+$ species were observed which suggested that ligand-exchange reactions can occur without the release of Al-containing etch species. Density functional theory (DFT) and coupled cluster singles, doubles, and perturbative triples (CCSD(T)) calculations were performed to support the preference for dimer products. The theoretical results confirmed the stability of the dimer products and showed that dimers with two Al−F−Al bridging bonds are the most stable and dimers with two Al−CH_3−Al bridging bonds are the least stable. In addition, the calculations suggested that dimers with terminal CH_3 ligands are most able to desorb from the surface because these dimers need to break weak Al−CH_3−Al bridging bonds. Transmission electron microscopy (TEM) studies confirmed the thermal Al_2O_3 ALE of Al_2O_3 films on W powders. The TEM images revealed that the etch process was uniform and conformal after various numbers of thermal Al_2O_3 ALE cycles using HF and TMA as the reactants.

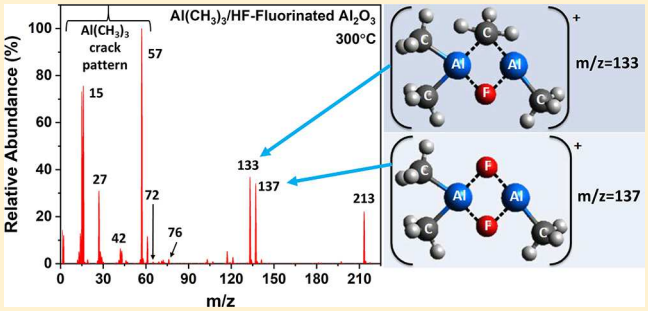

I. INTRODUCTION

Atomic layer etching (ALE) uses sequential, self-limiting surface reactions to remove material with atomic level precision.[1] Plasma and thermal ALE are two types of ALE. Plasma ALE is based on surface modification and then removal of the surface modified layer using energetic species via sputtering.[1] Plasma ALE yields anisotropic etching. In contrast, thermal ALE is based on thermal reactions and can remove material without the need of sputtering.[2] Thermal ALE can be viewed as the reverse of atomic layer deposition (ALD).[3,4] Thermal ALE and ALD are both isotropic processes that are needed for atomic layer processing. ALD is a mature technology with an origin many decades ago. Thermal ALE is a recent development that was discovered less than five years ago. The understanding of thermal ALE is still in its nascent stage.

The first thermal ALE was performed on Al_2O_3 using sequential fluorination and ligand-exchange reactions.[2,5] HF was the fluorination reactant, and $Sn(acac)_2$ was the metal precursor used for ligand exchange.[2,5] The thermal ALE of other materials, such as HfO_2 and AlN, was also developed using HF and $Sn(acac)_2$ as the reactants.[6,7] Subsequent work showed that thermal Al_2O_3 ALE could also be accomplished using HF and $Al(CH_3)_3$ (trimethylaluminum (TMA)).[8,9] This demonstration was significant because TMA is also the main metal precursor for Al_2O_3 ALD.[10] In addition, Al_2O_3 ALE or AlF_3 ALD could be obtained using HF and TMA depending on the substrate temperature.[8,11]

Other mechanisms for thermal ALE have also been discovered based on the conversion of the surface layer of the material.[12,13] After conversion, the new surface layer can be etched using fluorination and ligand exchange. The "conversion-etch" mechanism has been developed for thermal ZnO and SiO_2 ALE.[12,13] In addition, a variation of the "conversion-etch" mechanism was employed for thermal W ALE where the surface of W was first oxidized to a WO_3 layer.[14] Subsequently,

Received: July 2, 2019
Revised: November 23, 2019
Published: November 26, 2019

DOI: 10.1021/acs.jpcc.9b06104
J. Phys. Chem. C 2020, 124, 287−299

the WO_3 surface layer was converted to B_2O_3 using BCl_3 prior to the spontaneous etching of B_2O_3 to produce a volatile fluoride using HF.[14]

Oxidation was also used for thermal TiN ALE.[15] In this case, the surface of TiN was first oxidized to TiO_2 using ozone. The TiO_2 surface layer was then spontaneously etched by fluorination with HF to produce a volatile fluoride.[15] Thermal Si ALE is another version of oxidation and "conversion etch".[16] The silicon substrate is first oxidized to form a SiO_2 surface layer. Subsequently, the SiO_2 surface layer is converted to Al_2O_3 prior to the etching of Al_2O_3 using fluorination and ligand exchange.[16]

Other fluorination reactants besides HF have also been developed for thermal ALE. SF_4 was employed for thermal VO_2 ALE using SF_4 for fluorination and $Sn(acac)_2$ as the metal precursor for ligand exchange.[17] XeF_2 was used for thermal GaN ALE using XeF_2 for fluorination and BCl_3 for ligand exchange.[18] Other metal precursors have also been utilized for ligand exchange after the fluorination reaction during thermal ALE. $SiCl_4$ (silicon tetrachloride) and $TiCl_4$ (titanium tetrachloride) have been used together with HF for fluorination to achieve thermal ZrO_2 and HfO_2 ALE.[9,19] $AlCl(CH_3)_2$ (dimethylaluminum chloride, (DMAC)) has also been used together with HF for fluorination to obtain thermal ZrO_2 and HfO_2 ALE.[9]

Most of the understanding of thermal ALE has been derived from quartz crystal microbalance (QCM) measurements of film mass, Fourier transform infrared (FTIR) studies of surface species, and X-ray reflectivity (XRR) and spectroscopic ellipsometry (SE) investigations of film thickness. This previous work has established etch rates and identified the surface species after the various sequential reactions. The volatile etch products resulting from the sequential reactions have been inferred based on the surface chemistry. However, there has been no direct confirmation of the volatile etch products.

In this work, a custom-built reactor with *in situ* quadrupole mass spectrometry (QMS) was used to identify the volatile species produced during thermal ALE on powder samples. The QMS studies focused on thermal Al_2O_3 ALE using HF as the fluorination reactant. Various metal precursors were explored for the ligand-exchange reaction including TMA, DMAC, $SiCl_4$, and $TiCl_4$. Similar experiments were also conducted using AlF_3 to avoid using HF to fluorinate Al_2O_3. To confirm the QMS observations, density functional theory (DFT) and coupled cluster (CC) calculations were also performed on the possible etch products. In addition, transmission electron microscopy (TEM) was used to verify the thermal ALE of Al_2O_3 using HF and TMA.

II. EXPERIMENTAL SECTION

Thermal ALE Chemistry. The fluorination reaction during thermal Al_2O_3 ALE was studied using HF−pyridine (~30% pyridine, ~70% HF, Sigma-Aldrich) and 500 mg of Al_2O_3 powder (40−50 nm APS, Nanophase). The Al_2O_3 powder had a high surface area of 32−40 m^2/g to produce a large quantity of volatile reaction products. In addition, the high surface area of the Al_2O_3 powder greatly exceeded the surface area of the chamber walls. The ligand-exchange reactions on HF-fluorinated Al_2O_3 powder and AlF_3 powder (99.8%, Sigma-Aldrich) were performed using $Al(CH_3)_3$ (97%, Sigma-Aldrich), $SiCl_4$ (99%, Sigma-Aldrich), $TiCl_4$ (99.0% Sigma-Aldrich), and $AlCl(CH_3)_2$ (97%, Sigma-Aldrich) as the metal precursors.

In situ quadrupole mass spectrometry (QMS) analysis of the fluorination and ligand-exchange reactions was performed at 300 °C under static dosing conditions. The HF pressure was provided by a HF−pyridine solution.[20] The HF vapor pressure over the HF−pyridine solution was 90−100 Torr at room temperature.[7] The pyridine vapor pressure is also negligible.[21] For the fluorination reaction with Al_2O_3 powder, 9 Torr of HF was held statically in the reaction chamber for 60 s before purging. For the ligand-exchange reactions, 9 Torr of either $Al(CH_3)_3$, $SiCl_4$, $TiCl_4$, or $AlCl(CH_3)_2$ was also maintained in the chamber statically for 60 s. Every precursor exposure was followed by a purging sequence of 120 s of static purge, 240 s of viscous N_2 purge, and final 120 s of static purge to prevent cross-contamination between reactant precursors.

The QMS sampling was performed during the reactant exposures. At the onset of the reactant exposure, a pneumatic valve was opened between the reaction chamber and the QMS ionization region, and the QMS scans were repeated continuously for 60 s. Each QMS scan from m/z = 0 to 300 required 6 s. Ten scans were conducted during the 60 s exposure. The QMS spectra were largely unchanged after the second scan. The first scan could be affected by adsorbed gases on the powder sample and the chamber walls that are present after atmospheric exposures when loading the samples. The results shown in this paper were obtained from the eighth or ninth scan during the 60 s exposure.

Reactor for Quadrupole Mass Spectrometer (QMS) Analysis. The *in situ* QMS studies were performed in a custom reactor. The reactor consists of a stainless steel tube that is 1.5 in. diameter × 19 in. long (Figure 1A). A precursor manifold containing six precursor lines and one N_2 purge line is separated from the reaction chamber by a pneumatically actuated bellows valve to allow for static dosing and purging (Figure. 1B). To avoid cross-contamination, each precursor

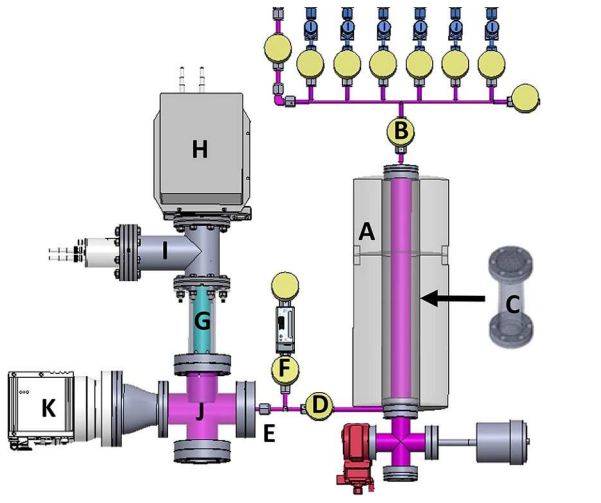

Figure 1. Schematic of ALE reactor with *in situ* QMS: (A) main reactor with ceramic heater; (B) valve separating precursor manifold from main reactor; (C) powder sample holder; (D) additional valve; (E) aperture separating reactor from ionizer region; (F) N_2 purging of aperture region with mass flow controller and valve; (G) QMS analyzer; (H) RF generator; (I) secondary electron multiplier; (J) differential-pumped ionizer region; and (K) turbomolecular pump.

DOI: 10.1021/acs.jpcc.9b06104
J. Phys. Chem. C 2020, 124, 287−299

line is purged with N_2 in isolation from the reaction chamber prior to using another precursor.

The Al_2O_3 and AlF_3 powder substrates are housed in a stainless steel mini-conflat nipple with stainless steel mesh spot-welded to each end (Figure 1C). The stainless steel mesh enables mass transport of the reactants to the powder surface while preventing the powder from dispersing in the reactor. The 1.33 in. outer diameter of the mini-conflat flange fits closely inside the 1.5 in. diameter reactor tube. The close contact of the mini-conflat flange with the reactor tube walls provides good thermal contact and ensures uniform heating of the powder sample.

An additional pneumatically actuated bellows valve separates the reaction chamber from the mass spectrometer ionization region (Figure 1D). A 100 μm diameter aperture is situated between this valve and the ionization region (Figure 1E). This aperture allows volatile etch products from the reactor at high pressures of ~1−10 Torr to be detected at low pressures of $\leq 1 \times 10^{-5}$ Torr in the ionization region. As etch species are produced during the reactant exposure, a gas stream flows through the 100 μm aperture to the ionizer and the ions are detected by QMS. An additional valve and mass flow controller are located between the aperture and the reaction chamber through a T-joint to allow separate N_2 purging of the aperture region (Figure 1F). This purging ensures that the reactants and product gases are completely removed from the aperture region between each reaction.

Detection of the volatile products was accomplished using a HiQuad QMG 700 QMS (Pfeiffer Vacuum). The HiQuad system is composed of the QMA 400 analyzer inside a 2.5 in. diameter stainless steel tube (Figure 1G) and the QMH 400-5 high-frequency generator (Figure 1H). The QMA 400 analyzer consists of a crossbeam ion source with two tungsten filaments, a quadrupole mass filter (8 mm diameter by 200 mm long molybdenum rods), and both Faraday and secondary electron multiplier detectors (Figure 1I).

The mass spectrometer analyzer is situated perpendicular to the incoming gas stream. The crossbeam ion source has an open design that allows quick response to changes in the gas composition. This geometry also minimizes exposure to the corrosive gas species and increases the signal-to-noise ratio for the volatile etch products. The QMH 440-5 RF generator provides a mass range of 1−512 amu necessary for the detection of large etch species with high sensitivity and resolution.

The QMS scans from m/z = 0 to 300 were performed continuously for 60 s during the reactant exposures. The scans were typically ended at m/z = 300 because the mass signals above m/z = 300 were negligible. The ionization region of the chamber (Figure 1J) and lines leading to the ionization region were maintained at 180 °C. This high temperature prevents condensation of the volatile etch products. The ionization region is pumped with a turbomolecular pump (Figure 1K).

Characterization of Thermal Al_2O_3 ALE Using TEM. Transmission electron microscopy (TEM) analysis was performed using an FEI Tecnai T12 instrument operated at 100 kV in bright field mode. The TEM characterized the thickness of Al_2O_3 films on W powder. The W powder was crystalline with particle sizes ranging from 0.6 to 1 μm (99.9%, Sigma-Aldrich). TEM images were obtained as the Al_2O_3 ALD films were progressively etched using sequential HF and $Al(CH_3)_3$ exposures at 300 °C. The TEM images revealed the uniformity and conformality of the Al_2O_3 films on the W powder.

Computational Details. Examination of the ligand-exchange reactions of HF-fluorinated Al_2O_3 and AlF_3 with $Al(CH_3)_3$, as well as the dimerization reactions, was performed using a combination of quantum chemical and thermochemical calculations. All calculations, unless otherwise noted, were performed using Gaussian 16.[22] Unrestricted DFT calculations were performed at the UMN15/6-31g level of theory[23] to optimize the molecular structures and determine the harmonic frequencies.[24,25]

Initial calculations were performed on one of the possible dimer products, di-μ-fluoridotetrafluoridodialuminum. These calculations showed that using tighter convergence tolerances for the SCF and geometry optimization changed the free energies results by <0.01 eV. As a result, the default convergence thresholds of 3×10^{-4} hartree/bohr for the root mean-squared (RMS) force per atom and 1.2×10^{-3} bohr for the RMS displacement per atom were used for all calculations reported in this work. Accurate energy calculations were performed using the unrestricted coupled cluster singles, doubles, and perturbative triples (UCCSD(T))/6-31g level of theory at the DFT optimized geometries.[26−29]

The structural and vibrational information from UMN15 calculations was used to calculate the thermal correction arising from translational, rotational, and vibrational degrees of freedom at finite temperature. For a detailed description of the methods used to calculate these contributions, see Chapter 11 in ref 30. The frequencies were scaled with a factor of 0.979 following previous instructions.[31] All calculations were performed on the RMACC Summit supercomputer.[32]

III. RESULTS AND DISCUSSION

Fluorination of Al_2O_3 Powder Using HF. H_2O is the predicted reaction product for the fluorination reaction of

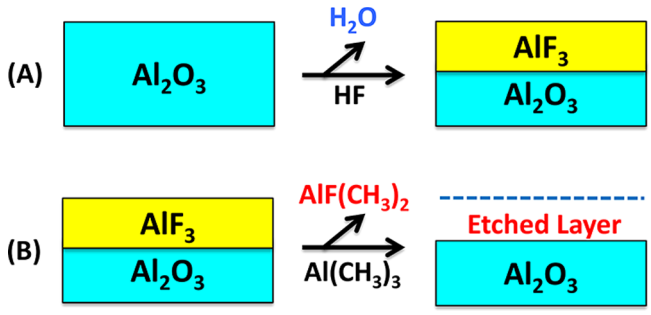

Figure 2. Proposed mechanism for Al_2O_3 thermal ALE based on sequential reactions using HF as the fluorination reactant and $Al(CH_3)_3$ as the metal precursor for ligand exchange.

Al_2O_3 with HF.[33] This reaction is shown in Figure 2 and can be written as

$$Al_2O_3(s) + 6HF(g) \rightarrow 2AlF_3(s) + 3H_2O(g) \quad (1)$$

To investigate this fluorination reaction using QMS, 500 mg of Al_2O_3 powder was exposed to 9 Torr of HF at 300 °C. Figure 3 shows the mass spectrum results for the products produced during the fluorination reaction.

As predicted by the proposed mechanism in Figure 2, the predominant reaction product observed in Figure 3 is H_2O^+ at m/z = 18. The presence of F^+ at m/z = 19 is also observed in

DOI: 10.1021/acs.jpcc.9b06104
J. Phys. Chem. C 2020, 124, 287−299

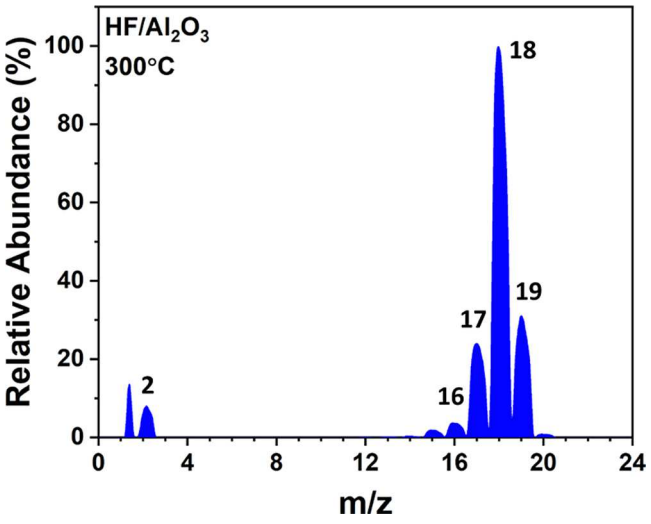

Figure 3. Mass spectrum showing ion signals after the fluorination of Al_2O_3 powder using HF at 300 °C.

Figure 3. The F^+ signal is the result of excess HF reactant during the static HF exposure. The peaks at m/z = 17 and m/z = 16 are identified as OH^+ and O^+, respectively, from the crack of H_2O^+. The *in situ* QMS results confirm that H_2O is the volatile reaction product from the fluorination of Al_2O_3 with HF.

Ligand Exchange between $Al(CH_3)_3$ and HF-Fluorinated Al_2O_3 Powder. $AlF(CH_3)_2$ (dimethylaluminum fluoride (DMAF)) is the predicted reaction product for the ligand-exchange reaction of $Al(CH_3)_3$ with AlF_3. This reaction is shown in Figure 2 and can be written as

$$AlF_3(s) + 2Al(CH_3)_3(g) \rightarrow 3AlF(CH_3)_2(g) \quad (2)$$

This ligand-exchange reaction was examined by exposing 9 Torr of $Al(CH_3)_3$ to the HF-fluorinated Al_2O_3 powder. To ensure a fully fluorinated Al_2O_3 surface, the Al_2O_3 powder was exposed to multiple HF exposures at 9 Torr for 60 s at 300 °C. Figure 4 shows the mass spectrum produced during this ligand-exchange reaction.

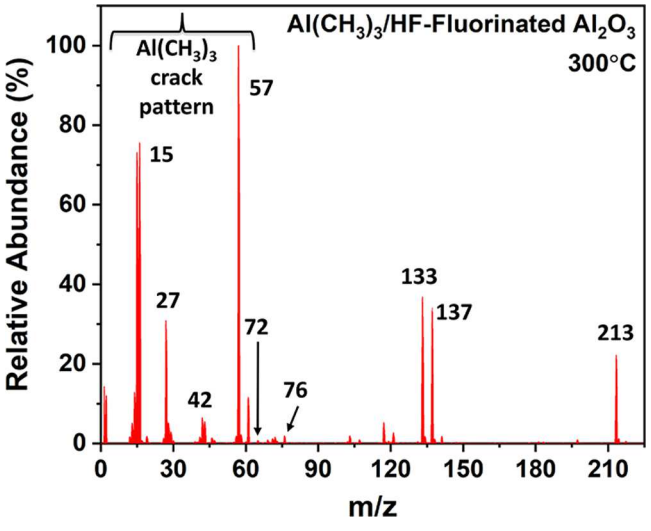

Figure 4. Mass spectrum showing ion signals after ligand-exchange between $Al(CH_3)_3$ and HF-fluorinated Al_2O_3 powder at 300 °C.

The peaks at m/z < 100 are almost all attributed to TMA and the fragmentation pattern of TMA. The mass signal at m/z = 15 is higher than expected from the TMA fragmentation pattern because TMA can produce CH_4 by reaction with HF on the surface of the HF-fluorinated Al_2O_3 powder.[8] The largest mass fragment is observed at m/z = 57 corresponding to $Al(CH_3)_2^+$. The peaks at m/z = 42, 27, and 15 correspond to $Al(CH_3)^+$, Al^+, and CH_3^+, respectively. The parent molecular ion is observed at m/z = 72 for $Al(CH_3)_3^+$ and has a small relative abundance of 1.7%. These peaks for $Al(CH_3)_3$ are observed because excess $Al(CH_3)_3$ reactant was used to ensure a complete reaction with the HF-fluorinated Al_2O_3 powder.

In addition to the mass peaks for the TMA reactant, the predicted product for the ligand-exchange reaction between TMA and AlF_3 is DMAF.[11] DMAF is believed to be the volatile etch product because DMAF has a vapor pressure of 80 Torr at 100 °C.[34] DMAF should be observed at m/z = 76. However, Figure 4 shows that only a very small signal is observed at m/z = 76. The peak at m/z = 76 has a low relative abundance of 1.9%.

Instead of observing a significant peak at m/z = 76 for DMAF, larger peaks at m/z = 133, 137, and 213 are observed in Figure 4. These peaks at m/z = 133, 137, and 213 correspond to the molecular ions $Al_2F(CH_3)_4^+$, $Al_2F_2(CH_3)_3^+$, and $Al_3F_3(CH_3)_5^+$, respectively. The peaks at m/z = 133 and 137 have approximately the same ion currents and are consistent with the ionization of dimers of DMAF with TMA (DMAF + TMA) or with itself (DMAF + DMAF). Each of these dimer ions has lost one CH_3 group from the original parent molecule. The peak at m/z = 213 corresponds to $Al_3F_3(CH_3)_5^+$. This peak could result from the ionization of $Al_3F_3(CH_3)_5$. This trimer etch product is similar to a trimer of DMAF that has lost one CH_3 group.

DMAF forms after two ligand-exchange reactions of TMA with AlF_3. $AlF_2(CH_3)$ could also form after one ligand-exchange reaction of TMA with AlF_3. A dimer formed from $AlF_2(CH_3)$ and TMA would have the same mass signature as a dimer formed from two DMAF molecules. The molecular ion at m/z = 137 corresponding to $Al_2F_2(CH_3)_3^+$ may originate from $AlF_2(CH_3)$ and TMA. However, Figure 4 shows that there is no signal observed at m/z = 80 for $AlF_2(CH_3)$. If the molecular ion at m/z = 137 is formed from $AlF_2(CH_3)$ and TMA, then no volatile $AlF_2(CH_3)$ desorbs by itself and appears in the mass spectrum.

Figure 5 shows the proposed structures for the molecular ions $Al_2F(CH_3)_4^+$, $Al_2F_2(CH_3)_3^+$, and $Al_3F_3(CH_3)_5^+$ at m/z = 133, 137, and 213, respectively. The bridge bonds between the Al metal centers are shown by the dashed lines.

The dimers and trimer of DMAF could form on the surface and then desorb as dimers and trimer. Alternatively, the dimers and trimers could form in the gas phase after DMAF desorbs as a monomer from the surface. To distinguish between these two possibilities, additional experiments were performed under different reaction conditions. The formation of the dimers and trimers in the gas phase should be more favorable at higher partial pressures of DMAF. Dimers and trimers should be less probable at much lower partial pressures of TMA and product DMAF.

Experiments were performed under viscous flow conditions at much lower TMA pressures. 500 mg of Al_2O_3 powder was initially fluorinated with HF to form an HF-fluorinated Al_2O_3 surface. TMA was then flowed continuously through the

DOI: 10.1021/acs.jpcc.9b06104
J. Phys. Chem. C 2020, 124, 287−299

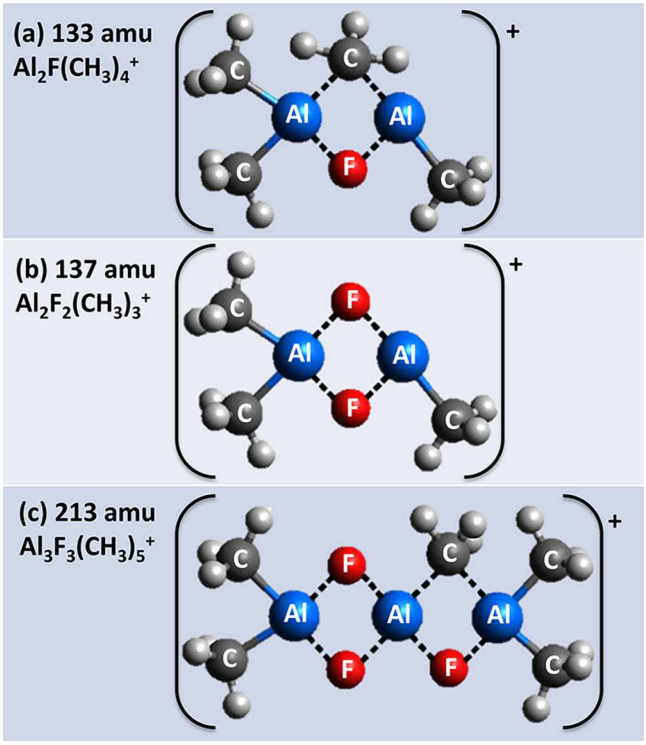

Figure 5. Proposed molecular structures of the main ions produced during the ligand-exchange reaction between $Al(CH_3)_3$ and HF-fluorinated Al_2O_3 powder at 300 °C.

reactor at a much lower pressure of 300 mTorr at 300 °C. The *in situ* QMS measurements showed the same ion signals for $Al_2F(CH_3)_4^+$, $Al_2F_2(CH_3)_3^+$, and $Al_3F_3(CH_3)_5^+$ at m/z = 133, 137, and 213, respectively. The ion currents were less than the ion currents during the static exposures. In addition, the ion current for the m/z = 137 peak was higher than the ion current for the m/z = 133 peak. The continued presence of the m/z = 133, 137, and 213 peaks at the much lower TMA pressure of 300 mTorr argues that these dimer and trimer products are forming on the surface prior to desorption rather than in the gas phase after the desorption of DMAF monomers. The larger ion current for the peak at m/z = 137 corresponding to the dimer of DMAF with itself (DMAF + DMAF) is also consistent with the expected higher ratio of the DMAF/TMA surface coverages at lower TMA pressure.

Dimers of TMA have been observed by previous studies. Because of the stability of CH_3 bridge bonding between the Al metal centers, trimethylaluminum is known to exist primarily as a dimer, $Al_2(CH_3)_6$, at lower temperatures and higher TMA pressures.[35] At higher temperatures, the dimer progressively dissociates into TMA monomers.[35,36] TMA is ~34% dissociated at 155 °C and 30 Torr.[36] TMA exists as more than 98% monomer at 215 °C and 30 Torr.[37]

The present experiments were performed at 300 °C and 9 Torr where TMA dimers dissociate into TMA monomers.[35] The absence of TMA dimers was verified by introducing TMA into the reactor with no HF-fluorinated Al_2O_3 powder. The QMS analysis did not reveal any TMA dimers from the reactor at 300 °C. In contrast, incorporation of a halogen into the bridging position in an Al_2 dimer increases the stability of the Al_2 dimer. For example, the Al−Cl−Al bridging bond in the dimethylaluminum chloride (DMAC) dimer is preferred compared with the Al−CH_3−Al bridging bond.[38] No measurable dissociation of the DMAC dimer was measured at 92−155 °C.[39]

$AlCl_3$ also has a stable Al_2Cl_6 dimer because of strong Al−Cl−Al bridge bonding. Al_2Cl_6 is observed as the sublimation product from solid $AlCl_3$ by mass spectrometry studies.[40] Gas phase electron diffraction studies also identify Al_2Cl_6 as the evaporation product from solid $AlCl_3$.[41] In addition, $AlCl_3$ will form volatile dimer complexes with a range of metal chlorides.[40,42,43] $AlCl_3$ is also used extensively in chemical vapor transport reactions to purify various metal complexes.[44] Many volatile dimeric and polymeric metal chloride complexes form with $AlCl_3$ because of strong chlorine−bridge linkages.[45,46] In addition, AlF_3 has a polymeric structure and a high melting temperature of 1290 °C. The AlF_3 dimer, Al_2F_6, has been observed using mass spectrometry at 752 °C.[47] The strengths of the two Al−F−Al bridging bonds are capable of maintaining an Al_2 dimer at elevated temperatures.

The presence of $Al_2F(CH_3)_4^+$, $Al_2F_2(CH_3)_3^+$, and $Al_3F_3(CH_3)_5^+$ molecular ions in the mass spectrum suggests that their dimer and trimer parents desorb from the HF-fluorinated Al_2O_3 powder. The proposed dimeric and trimeric products are supported by the observation that DMAF exists as a tetramer after leaving a gas nozzle at 80 °C.[48] DMAF also is detected as a tetramer in freezing benzene.[34] There is a possibility that the dimer and trimer molecular ions are derived from larger multimers of DMAF. However, the possible molecular ions at higher mass that would be consistent with a tetramer or other multimer were negligible.

Ligand-Exchange Reaction between $Al(CH_3)_3$ and AlF_3. The fluorination of Al_2O_3 with HF produces a surface layer of AlF_3 or AlO_xF_y oxyfluorides.[33,49] The previous section explored the ligand-exchange reaction between $Al(CH_3)_3$ and HF-fluorinated Al_2O_3 powder. For a comparison of the ligand-exchange reaction on HF-fluorinated Al_2O_3 and AlF_3, experiments can be performed using AlF_3 powder. Substituting AlF_3 powder for HF-fluorinated Al_2O_3 powder avoids the HF fluorination of Al_2O_3. The AlF_3 powder can also reveal the differences between the ligand exchange of $Al(CH_3)_3$ on AlF_3 and HF-fluorinated Al_2O_3 that may contain a surface layer of AlF_3 or AlO_xF_y oxyfluorides.[33,49]

The reaction of TMA with AlF_3 powder was performed in the same manner as the reaction of $Al(CH_3)_3$ with HF-fluorinated Al_2O_3 powder. 500 mg of AlF_3 powder was placed in the stainless steel mini-conflat nipple and contained by the stainless steel mesh. The AlF_3 powder was exposed to TMA at a pressure of 9 Torr at 300 °C. The volatile products were then detected by the *in situ* QMS using the same conditions employed for the HF-fluorinated Al_2O_3 powder.

The comparison of the ions detected after the ligand-exchange reaction of TMA with HF-fluorinated Al_2O_3 or AlF_3 is displayed in Figure 6. Figure 6a shows the molecular ions detected during the ligand exchange between TMA and HF-fluorinated Al_2O_3 powder. Figure 6b shows the molecular ions detected during the ligand exchange between TMA and AlF_3 powder. The two mass spectra are very similar. The ion signal at m/z = 15 corresponding with CH_3^+ is larger for TMA reacting with the HF-fluorinated Al_2O_3 powder in Figure 6a compared with TMA reacting with the AlF_3 powder in Figure 6b. The residual HF present in the chamber after HF exposures to form HF-fluorinated Al_2O_3 may react with TMA to produce additional CH_4. In addition, the same ions consistent with the ionization of dimer products at m/z = 133 and 137 and trimer products m/z = 213 are produced when

DOI: 10.1021/acs.jpcc.9b06104
J. Phys. Chem. C 2020, 124, 287−299

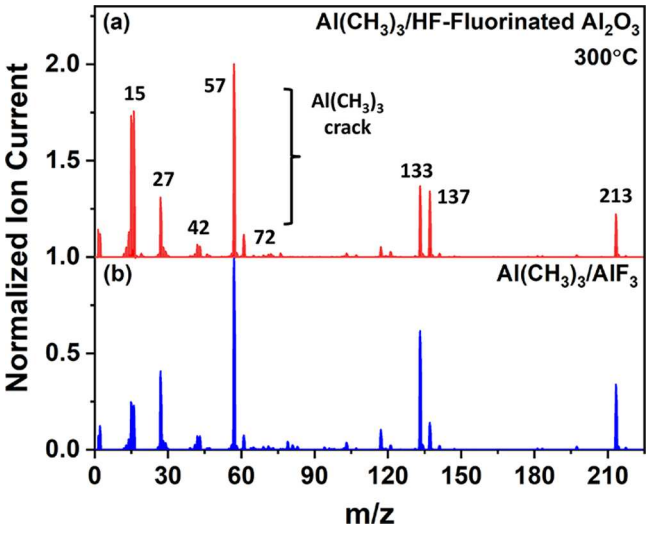

Figure 6. Comparison of the mass spectra after (a) reaction of $Al(CH_3)_3$ with HF-fluorinated Al_2O_3 powder at 300 °C and (b) reaction of $Al(CH_3)_3$ with AlF_3 powder at 300 °C.

TMA reacts with either HF-fluorinated Al_2O_3 powder or AlF_3 powder.

The ion at m/z = 133 is slightly larger relative to the ion at m/z = 137 for the results from HF-fluorinated Al_2O_3 powder in Figure 6a. In contrast, the ion at m/z = 133 is much larger relative to the ion at m/z = 137 for the results from AlF_3 powder in Figure 6b. The differences between m/z = 133 and m/z = 137 for the HF-fluorinated Al_2O_3 powder in Figure 6a and the AlF_3 powder in Figure 6b may result from the difference between the AlF_3 or AlF_xO_y layer on the HF-fluorinated Al_2O_3 powder[33,49] and the AlF_3 surface of the AlF_3 powder. The AlF_3 powder is crystalline. This crystallinity may slow down the etching and lead to a larger TMA to DMAF ratio in the reactor. More TMA relative to DMAF would be expected to increase the ion signal at m/z = 133 derived from the dimer of DMAF with TMA (DMAF + TMA).

Figure 6b also shows that TMA reactant remains in the gas phase in the presence of AlF_3 powder. All of the TMA is not reacted by the AlF_3 powder. This observation indicates that the ligand-exchange reaction between TMA and AlF_3 becomes self-limiting under these reaction conditions. Subsequent TMA exposures to the same AlF_3 powder after purging the reactor led to equivalent results as displayed in Figure 6b. These results suggest that the surface species that limit the etching of AlF_3 by TMA must be released during the purging process.

The close agreement between the results for HF-fluorinated Al_2O_3 powder and AlF_3 powder in Figure 6 indicates that AlF_3 powder can be used as a substitute for the HF-fluorinated Al_2O_3 powder. The fluorination of Al_2O_3 powder using HF is not necessary to produce fluorinated Al_2O_3 to study ligand-exchange reactions. Consequently, the remainder of the ligand-exchange studies will utilize AlF_3 powder to study the ligand-exchange reaction between $AlCl(CH_3)_2$, $SiCl_4$, and $TiCl_4$ and fluorinated Al_2O_3.

Ligand-Exchange Reaction between $AlCl(CH_3)_2$ and AlF_3. Thermal Al_2O_3 ALE can be performed using HF and $AlCl(CH_3)_2$ (dimethylaluminum chloride (DMAC)) as the reactants.[9] To understand the differences between DMAC and TMA, DMAC was explored as the metal precursor for the ligand-exchange reaction with AlF_3. For these *in situ* QMS experiments, 500 mg of AlF_3 powder was placed in the stainless steel mini-conflat sample holder and exposed to 9 Torr of $AlCl(CH_3)_2$ at 300 °C. Figure 7 shows the QMS results. The

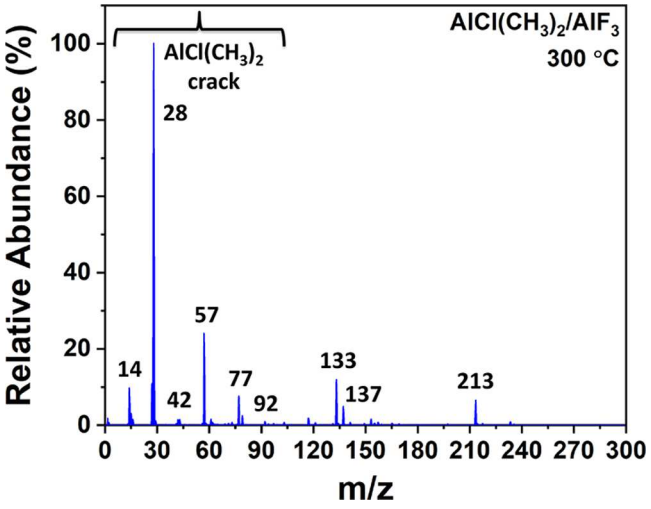

Figure 7. Mass spectrum showing ion signals after ligand exchange between $AlCl(CH_3)_2$ and AlF_3 powder at 300 °C.

large peak at m/z = 28 amu is from the fragmentation of $AlCl(CH_3)_2$ and is attributed to AlH^+. Peaks at m/z = 92, 57, 42, and 14 are also associated with the cracking pattern for $AlCl(CH_3)_2$.

In addition to the mass peaks for $AlCl(CH_3)_2$ and its fragmentation pattern, sizable peaks are also observed at m/z = 133, 137, and 213 in Figure 7. The peaks at m/z = 133 and 137 correspond to the $Al_2F(CH_3)_4^+$ and $Al_2F_2(CH_3)_3^+$ molecular ions. The peak at m/z = 213 corresponds to the $Al_3F_3(CH_3)_5^+$ molecular ion. These peaks are in agreement with the spectra in Figures 4 and 6 for the ligand exchange of TMA with either HF-fluorinated Al_2O_3 or AlF_3. The similarity of the results for TMA and DMAC argues that the dominant ligand-exchange reaction is the ligand transfer of CH_3 from either TMA or DMAC to AlF_3.

There are also some mass peaks that are consistent with ligand transfer of Cl from DMAC to AlF_3. Figure 8 shows an expanded scale of the mass spectrum from m/z = 150 to m/z = 300 amu after the ligand-exchange reaction between DMAC and AlF_3. The peak at m/z = 153 corresponds to the ionization of the $Al_2FCl(CH_3)_4$ dimer to produce the $Al_2FCl(CH_3)_3^+$ molecular ion after losing one CH_3 group. The peak at m/z = 157 corresponds to the ionization of the $Al_2F_2Cl(CH_3)_3$ dimer to produce the $Al_2F_2Cl(CH_3)_2^+$ molecular ion after losing one CH_3 group. The $Al_2FCl(CH_3)_3^+$ and $Al_2F_2Cl(CH_3)_2^+$ ions have relative abundances of 1.55% and 0.75%, respectively. The peak at m/z = 233 is believed to correspond to the ionization of the $Al_3F_3Cl(CH_3)_4$ trimer to produce the $Al_3F_3Cl(CH_3)_4^+$ molecular ion. These assignments were confirmed by the natural isotopic abundances for chlorine. The isotopic distributions were generated using the Scientific Instrument Services, Inc., isotope distribution calculator. The proposed structures of these molecular ions are shown in Figure 9. The bridge bonds between the Al metal centers are again shown by the dashed lines.

Additional smaller peaks are also present in Figure 8. The peak clusters at m/z = 165, 169, 173, and 177 correspond to molecular ions from mixed-oxy-halogen dimers. These ions are

DOI: 10.1021/acs.jpcc.9b06104
J. Phys. Chem. C 2020, 124, 287−299

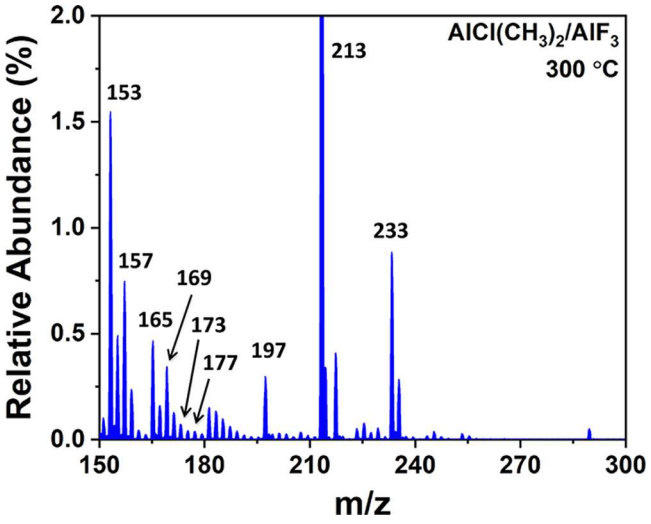

Figure 8. Expansion of region of mass spectrum in Figure 7 from m/z = 150−300 to highlight mixed-halogen etch products.

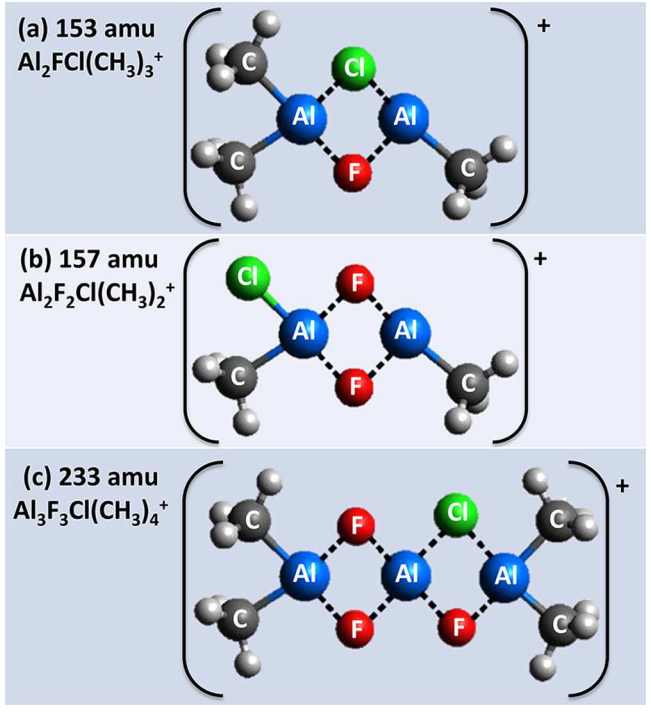

Figure 9. Proposed molecular structures of the ions of the mixed-halogen etch products produced during the ligand-exchange reaction between $AlCl(CH_3)_2$ and AlF_3 powder at 300 °C.

attributed to $Al_2OCl(CH_3)_4^+$ at m/z = 165, $Al_2OFCl(CH_3)_3^+$ at m/z = 169, $Al_2F_2OCl(CH_3)_2^+$ at m/z = 173, and $Al_2F_3OCl(CH_3)^+$ at m/z = 177. The AlF_3 powder likely contains a surface oxide that provides the oxygen for these mixed-oxy-halogen dimers. These species were not observed earlier after TMA exposures on AlF_3 powder. Therefore, chlorine from DMAC may be necessary to form these mixed-oxy-halogen dimers. There are also small peaks at m/z = 181, 183, 185, 187, and 197 that may be derived from fragments of larger mixed-halogen trimers.

Reaction between $SiCl_4$ and $TiCl_4$ with AlF_3. Previous studies have revealed that $SiCl_4$ and $TiCl_4$ are unable to etch HF-fluorinated Al_2O_3.[9,19] These results were explained by reaction thermochemistry. The ligand-exchange reaction between $SiCl_4$ and AlF_3 is not thermochemically favorable. The reaction $^4/_3AlF_3 + SiCl_4(g) \rightarrow {}^4/_3AlCl_3(g) + SiF_4(g)$ has a positive standard free energy change of ΔG° = +29 kcal at 300 °C.[50] Similarly, the ligand-exchange reaction between $TiCl_4$ and AlF_3 is also thermochemically unfavorable. The reaction $^4/_3AlF_3 + TiCl_4(g) \rightarrow {}^4/_3AlCl_3(g) + TiF_4(g)$ has a positive standard free energy change of ΔG° = +71 kcal at 250 °C.[50] The reactions of $SiCl_4$ and $TiCl_4$ with AlF_3 were explored using *in situ* QMS studies to confirm that $SiCl_4$ and $TiCl_4$ do not yield Al-containing etch products during ligand-exchange reactions with AlF_3.

The experiments were performed by placing 500 mg of AlF_3 powder in the stainless steel mini-conflat sample holder. The AlF_3 powder was then exposed to 9 Torr of $SiCl_4$ at 300 °C. Figure 10a shows the mass spectrum of $SiCl_4$ in the reactor

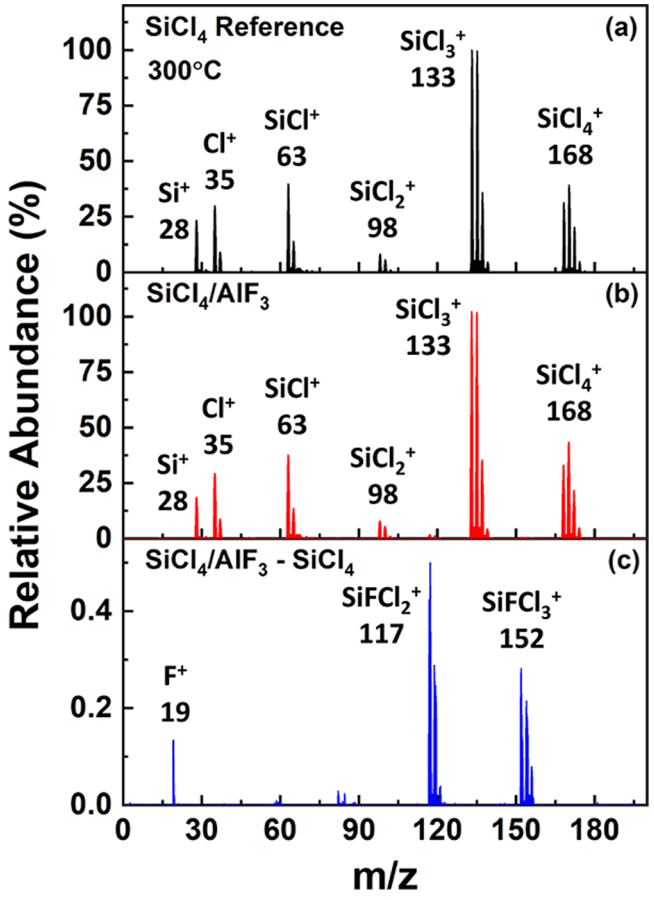

Figure 10. (a) Mass spectrum of $SiCl_4$ in reactor with no AlF_3. (b) Mass spectrum after ligand-exchange reaction between $SiCl_4$ and AlF_3 powder at 300 °C. (c) Mass spectrum from (b) with the $SiCl_4$ mass spectrum removed using peak at m/z = 133 for reference.

with no AlF_3 powder. This mass spectrum is equivalent to the reference spectrum for $SiCl_4$ from the NIST database. The mass spectrum after $SiCl_4$ exposure to the AlF_3 powder is shown in Figure 10b. The results in Figure 10b are nearly equivalent to the mass spectrum for $SiCl_4$ in Figure 10a. The natural isotopic abundances for both chlorine and silicon affect the mass spectrum for $SiCl_4$.

No peaks corresponding to Al-containing etch products were observed in the mass spectrum in Figure 10b. These results are consistent with the previous reports that $SiCl_4$ does

DOI: 10.1021/acs.jpcc.9b06104
J. Phys. Chem. C 2020, 124, 287−299

not etch HF-fluorinated Al_2O_3.[9] Although there are no Al-containing reaction products, there are some additional smaller peaks in Figure 10b that are not in the mass spectrum of $SiCl_4$. Figure 10c shows the mass spectrum in Figure 10b with the mass spectrum for $SiCl_4$ removed using the peak at m/z = 133 for calibration. The removal of the $SiCl_4$ mass spectrum reveals two clusters of peaks at m/z = 117 and m/z = 152.

The peaks in the cluster at m/z = 152 correspond to $SiFCl_3^+$. These peaks could be formed by a single ligand-exchange reaction between $SiCl_4$ and the AlF_3 surface. This ligand transfer between $SiCl_4$ and AlF_3 would also form $AlClF_2$ on the surface. This ligand-exchange product is not volatile. There are also peaks in the mass spectrum in Figure 10c in a cluster at m/z = 117. This cluster corresponds to $SiFCl_2^+$. The $SiFCl_2^+$ is likely the result of $SiFCl_3^+$ fragmentation. $SiFCl_3$ and HCl could also be formed by the reaction of $SiCl_4$ with residual HF in the reactor. However, there is no mass signal at m/z = 35 or 37 in Figure 10c after the removal of the $SiCl_4$ mass spectrum.

Experiments were also performed for $TiCl_4$ interacting with AlF_3. Similar to $SiCl_4$, $TiCl_4$ does not produce Al-containing etch products. However, there are halogen-exchange species formed by reaction with the AlF_3 surface. Figure 11a shows the mass spectrum for $TiCl_4$ in the reactor with no AlF_3 powder. This mass spectrum matches the reference spectrum for $TiCl_4$ in the NIST database. Figure 11b shows the mass spectrum after exposing 500 mg of AlF_3 powder to 9 Torr of $TiCl_4$ at 250 °C. The main species observed in Figure 11b are from $TiCl_4$ and its respective fragments. The natural isotopic abundances for both chlorine and titanium lead to the mass clusters observed in the mass spectrum for $TiCl_4$.

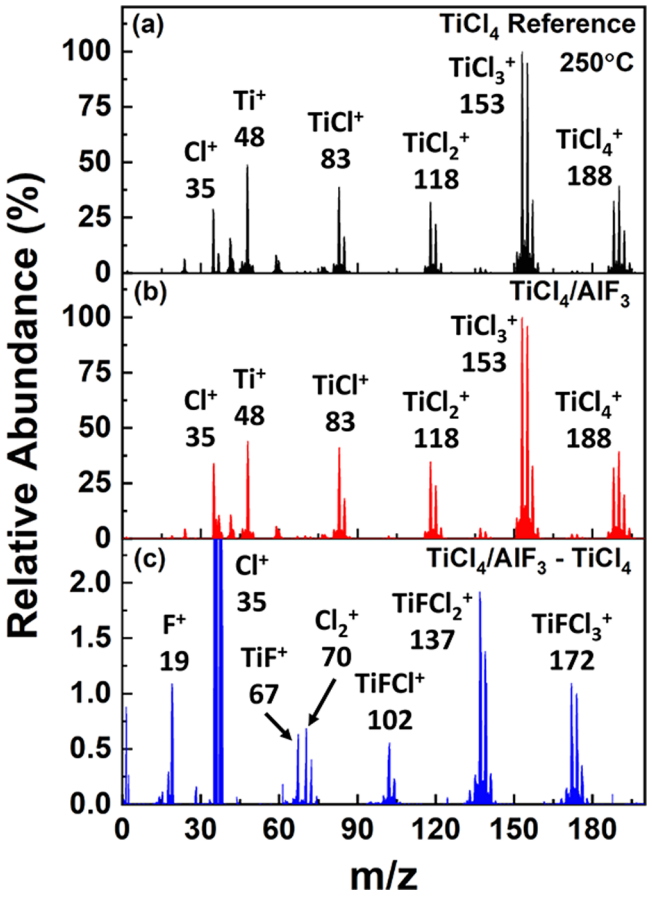

Figure 11. (a) Mass spectrum of $TiCl_4$ in reactor with no AlF_3. (b) Mass spectrum after ligand-exchange reaction between $TiCl_4$ and AlF_3 powder at 300 °C. (c) Mass spectrum from (b) with the $TiCl_4$ mass spectrum removed using the peak at m/z = 153 for reference.

Figure 11c shows the mass spectrum in Figure 11b with the mass spectrum for $TiCl_4$ removed using the peak at m/z = 153 for calibration. The removal of the $TiCl_4$ mass spectrum reveals peaks associated with $TiFCl_3$ resulting from a single ligand-exchange reaction between $TiCl_4$ and the AlF_3 surface. The cluster of peaks at m/z = 172 is assigned to $TiFCl_3^+$. Subsequent fragmentation of $TiFCl_3^+$ yields clusters of peaks at m/z = 137, 102 and 70, corresponding to $TiFCl_2^+$, $TiFCl^+$, and Cl_2^+, respectively. Additional peaks at m/z = 67 and 19 correspond to TiF^+ and F^+, respectively.

Characterization of Thermal Al_2O_3 ALE Using Transmission Electron Microscopy (TEM). TEM was used to confirm that HF and $Al(CH_3)_3$ etch Al_2O_3 at 300 °C. 100 cycles of Al_2O_3 ALD was first deposited on W powder using static exposures of $Al(CH_3)_3$ and H_2O at 200 °C. The static exposures were at 9 Torr for 60 s. The sample was then removed and imaged using TEM. The 100 cycles of Al_2O_3 ALD resulted in ~16 nm of conformal Al_2O_3 on the W particles as shown in Figure 12a.

The reactor temperature was then increased to 300 °C, and 50 cycles of thermal Al_2O_3 ALE was performed using 9 Torr and 60 s static exposures of HF and $Al(CH_3)_3$. The resulting products were monitored using *in situ* QMS. The products were consistent with the products previously observed while etching the HF-fluorinated Al_2O_3 powder as displayed in Figure 4. The powder sample was then removed from the reactor and imaged using TEM. After 50 thermal Al_2O_3 ALE cycles, the thickness of the Al_2O_3 coating was reduced to a thickness of ~13 nm as shown by the TEM image in Figure 12b. The Al_2O_3 thickness is still smooth and conformal on the W powder. The conformality demonstrates that the thermal Al_2O_3 ALE is isotropic on these Al_2O_3 films on the W powder.

The same sample was placed back into the reactor and exposed to another 50 cycles of thermal Al_2O_3 ALE cycles at 300 °C. The Al_2O_3 coating was further reduced to a thickness of ~5 nm as displayed by the TEM image in Figure 13a. The Al_2O_3 thickness remains smooth and conformal on the W powder, consistent with isotropic thermal Al_2O_3 ALE. The same sample was placed back into the reactor and exposed to another 50 cycles of thermal Al_2O_3 ALE cycles at 300 °C. After these additional cycles, the Al_2O_3 coating was completely removed by the thermal Al_2O_3 ALE as displayed by the TEM image in Figure 13b.

Computational Analysis. Calculations were performed to investigate the stability of the proposed $Al_2F(CH_3)_5$ and $Al_2F_2(CH_3)_4$ dimer products compared with the monomer products. The reaction of $Al(CH_3)_3$ with AlF_3 was initially studied to determine whether an activation barrier was present during ligand exchange and whether the ligand-exchange reaction was energetically favorable. A schematic of this reaction is shown in Figure 14. The free energy difference, ΔG, at T = 300 °C was calculated between the $Al(CH_3)_3$ and AlF_3 reactants and the predicted monomer products. The monomer products were DMAF and $AlF_2(CH_3)$. The free energy difference was also calculated between the $Al(CH_3)_3$ and AlF_3 reactants and the intermediate during the ligand-exchange reaction.

The DFT structural optimizations did not reveal an activation barrier between the reactants and products. The

DOI: 10.1021/acs.jpcc.9b06104
J. Phys. Chem. C 2020, 124, 287−299

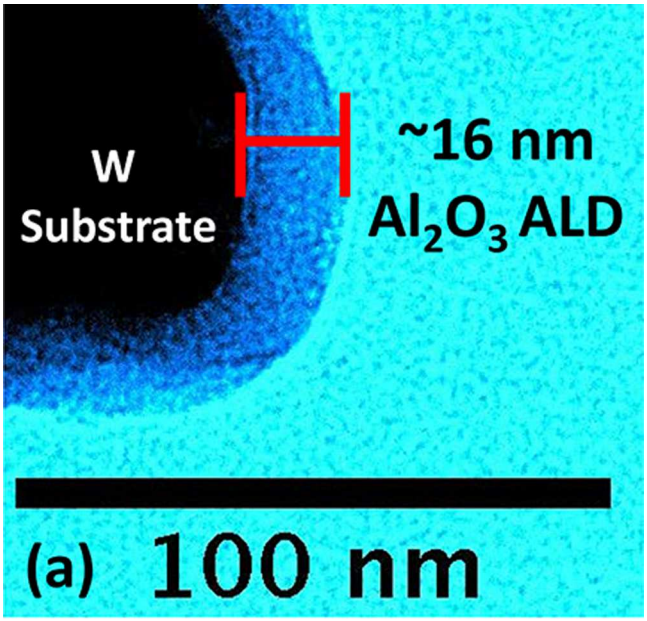

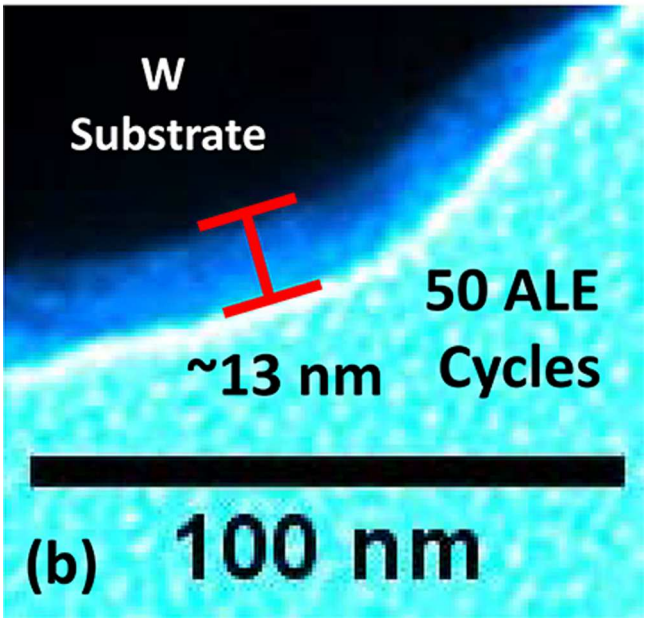

Figure 12. TEM images of (a) Al_2O_3 ALD film on W particle with initial thickness of ~16 nm and (b) Al_2O_3 film after 50 cycles of thermal Al_2O_3 ALE at 300 °C using HF and TMA as the reactants.

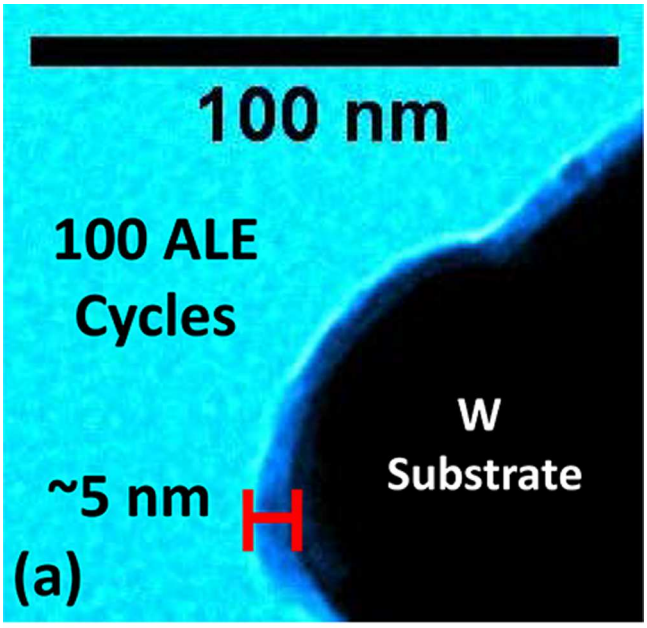

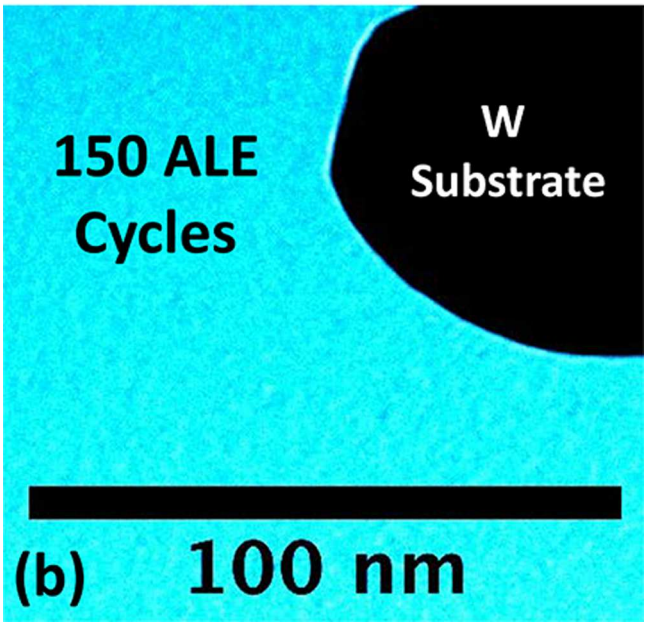

Figure 13. TEM images of (a) Al_2O_3 film after an additional 50 cycles of thermal Al_2O_3 ALE at 300 °C using HF and TMA as the reactants and (b) Al_2O_3 film after an additional 50 cycles of thermal Al_2O_3 ALE at 300 °C.

thermochemistry calculations determined that the intermediate dimer complex between TMA and AlF_3 during ligand exchange is lower in free energy than the AlF_3 and $Al(CH_3)_3$ reactants by $\Delta G(300\ ^\circ C) = -0.763$ eV as shown in Figure 14. The intermediate dimer complex during ligand exchange is shown prior to any rearrangement. In comparison, the $AlF(CH_3)_2$ and $AlF_2(CH_3)$ monomer products are lower in free energy than the AlF_3 and $Al(CH_3)_3$ reactants by $\Delta G(300\ ^\circ C) = -0.678$ eV. The intermediate dimer complex is lower in free energy than the monomer products by $\Delta G(300\ ^\circ C) = -0.085$ eV.

These results are consistent with the QMS observation of volatile dimer species as the main products during the ligand-exchange reaction between TMA and AlF_3. The rearrangement of F atoms and CH_3 groups within the intermediate dimer complex may also lead to free energies for isomers that are even lower than $\Delta G(300\ ^\circ C) = -0.763$ eV shown in Figure 14. These more stable dimer complexes are even more likely to favor the observation of volatile dimer species as etch products.

Theoretical calculations were used to examine the stability of all possible structures formed from the dimerization of the products from the reaction between AlF_3 and $Al(CH_3)_3$. The possible dimer structures are shown in Figure 15. Their $\Delta G(300\ ^\circ C)$ values and identifying names are given in Table 1. The ΔG values at 300 °C for all dimers were calculated by stoichiometrically balancing the starting reactants, AlF_3 and $Al(CH_3)_3$, and the given dimer. In other words, X and Y were determined for the general reaction $XAlF_3 + YAl(CH_3)_3 \rightarrow$ dimer in question. As an explicit example, the balanced

DOI: 10.1021/acs.jpcc.9b06104
J. Phys. Chem. C 2020, 124, 287−299

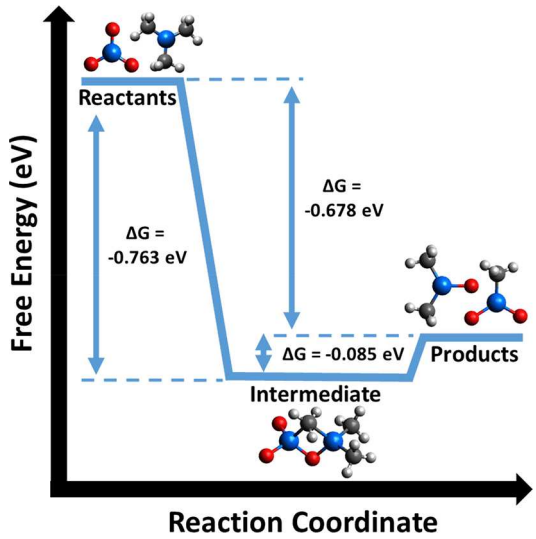

Figure 14. Free energy diagram showing reactants, the intermediate dimer complex, and products for ligand-exchange reaction between $Al(CH_3)_3$ and AlF_3. ΔG values were calculated using optimized geometries and frequencies from UMN15 with energies from UCCSD(T).

reaction for the formation of the $Al_2F_2(CH_3)_4$ dimer in Figure 15g is $^2/_3AlF_3 + {}^4/_3Al(CH_3)_3 \rightarrow Al_2F_2(CH_3)_4$.

Organizing all the possible dimer combinations by terminal groups and bridging pairs revealed interesting correlations. The dimer molecules containing fluorine bridge bonds were significantly more stable than those containing methyl bridge bonds. This trend is consistent with the ability of fluorine to form bimetallic bridge bonds.[51] The free energy of formation for dimers grows more positive, i.e., unfavorable, with the addition of each methyl bridging ligand. This instability is partially caused by the entropic cost of immobilizing methyl ligands in the bridging positions.

The observation of volatile products will be dependent on the stability of the dimer and the ability of the dimer to leave

Table 1. Possible Dimers versus Number of F and CH_3 Species for All Possible Structures of F and CH_3 in Bridge or Terminal Positions[a]

identifier	ΔG (eV)	name
a	−1.77	di-μ-fluoridotetrafluoridodialuminum
b	−2.05	di-μ-fluoridomethyltrifluoridodialuminum
c	−1.96	di-μ-fluoridodimethylaluminum−difluoridoaluminum
d	−2.24	di-μ-fluorido-*cis*-dimethylfluoridoaluminum
e	−2.18	di-μ-fluorido-*trans*-dimethylfluoridoaluminum
f	−2.01	di-μ-fluoridotrimethylfluoridodialuminum
g	−1.73	di-μ-fluoridotetramethyldialuminum
h	−0.70	μ-methyl-μ-fluoridotetrafluoridodialuminum
i	−0.83	μ-methyl-μ-fluoridomethyltrifluoridodialuminum
j	−0.76	μ-methyl-μ-fluoridodimethylaluminum−difluoridoaluminum
k	−0.81	μ-methyl-μ-fluorido-*cis*-dimethylfluoridoaluminum
l	−0.76	μ-methyl-μ-fluorido-*trans*-dimethylfluoridoaluminum
m	−0.80	μ-methyl-μ-fluoridotrimethylfluoridodialuminum
n	−0.10	μ-methyl-μ-fluoridotetramethyldialuminum
o	0.30	di-μ-methyltetrafluoridodialuminum
p	0.31	di-μ-methylmethyltrifluoridodialuminum
q	0.55	di-μ-methyldimethylaluminum−difluoridoaluminum
r	0.43	di-μ-methyl-*cis*-dimethylfluoridoaluminum
s	0.47	di-μ-methyl-*trans*-dimethylfluoridoaluminum
t	0.79	di-μ-methyltrimethylfluoridodialuminum
u	1.29	di-μ-methyltetramethyldialuminum

[a]The identifier refers to Figure 15. ΔG is the free energy of formation of the dimer from the AlF_3 and $Al(CH_3)_3$ reactants.

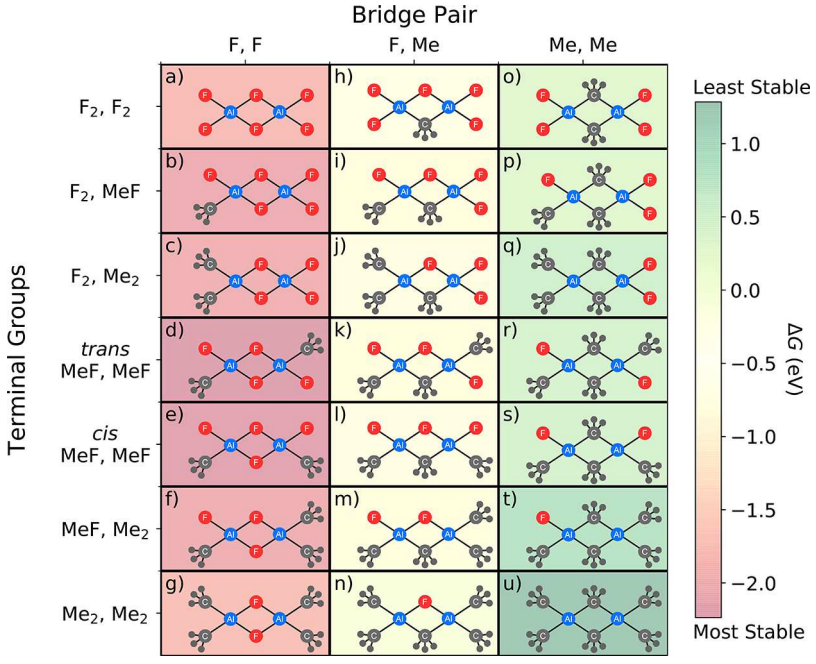

Figure 15. All possible dimer structures and their respective ΔG values organized by bridging pairs and terminal groups. The ΔG values were determined by subtracting the free energies of the AlF_3 and $Al(CH_3)_3$ reactants, multiplied by the appropriate stoichiometric coefficients, from the free energy of the dimer product. For example, the balanced reaction for the formation of the $Al_2F_2(CH_3)_4$ dimer in Figure 15g is $^2/_3AlF_3 + {}^4/_3Al(CH_3)_3 \rightarrow Al_2F_2(CH_3)_4$.

DOI: 10.1021/acs.jpcc.9b06104
J. Phys. Chem. C 2020, 124, 287−299

the surface. The Al_2F_6 dimer species displayed in Figure 15a (di-μ-fluorido-tetrafluoridodialuminum) is unlikely to be observed under the thermal Al_2O_3 ALE reaction conditions. AlF_3 has a high melting temperature of 1290 °C. This high stability is attributed to the strong Al−F−Al bridge bonding between AlF_3 molecules. The fully fluorinated terminal positions of the Al_2F_6 dimer will also have Al−F−Al bonds to surface Al atoms. The strength of these Al−F−Al bonds will hinder the desorption of the Al_2F_6 dimer.

The $Al_2(CH_3)_6$ dimer species illustrated in Figure 15u (di-μ-methyl-tetramethyldialuminum) is also not likely to be observed under the thermal Al_2O_3 ALE reaction conditions. The Al−CH_3−Al bridge bonding between $Al(CH_3)_3$ molecules is much weaker than Al−F−Al bridge bonding. The $Al_2(CH_3)_6$ dimer species is also not stable at higher temperatures.[35]

The expected volatile products are dimers with Al−F−Al bridge bonds and CH_3 ligands in the terminal positions. The Al−F−Al bridge bonds lead to dimer stability. The CH_3 ligands in the terminal positions enable the dimer to leave the surface. Based on these two observations, the ideal dimer with both stability and the ability to leave the surface would be $Al_2F_2Me_4$ illustrated in Figure 15g (di-μ-fluorido-tetramethyl-dialuminum).

Figure 15 can also illustrate how rearrangement of F atoms and CH_3 groups within a dimer complex to form various isomers can lead to lower free energies. For example, the F atoms and CH_3 groups in $AlF_2(CH_3)_4$ can be arranged to yield Figure 15s (di-*m*-methyl-*trans*-dimethylfluoridoaluminum), Figure 15m (*m*-methyl-*m*-fluoridotrimethylfluorido-dialuminum), or Figure 15g (di-*m*-fluorido-tetramethyl-dialuminum). The free energies of these isomers shown in Figures 15s, 15m, and 15g are $\Delta G(300\ °C) = +0.47$, −0.80, and −1.73 eV, respectively. During rearrangement from Figure 15s to Figure 15g, the F atoms will move to obtain the more stable bridging positions in the dimer.

The ion currents of the various observed dimers are consistent with dimers that have Al−F−Al bridge bonds and CH_3 ligands in the terminal positions. Figure 16 shows the ion currents for the dimers for the ligand-exchange reaction between TMA and HF-fluorinated Al_2O_3 surface at 300 °C as a function of number of CH_3 groups in the dimer. The dashed line is intended only to guide the eye. The F is always placed in an Al−F−Al bridge bond prior to a terminal position in the dimer. The lowest ion signal is for Al_2F_6 displayed in Figure 15a (di-μ-fluorido-tetrafluoridodialuminum). This dimer can not easily leave the surface because of strong Al−F−Al bonds.

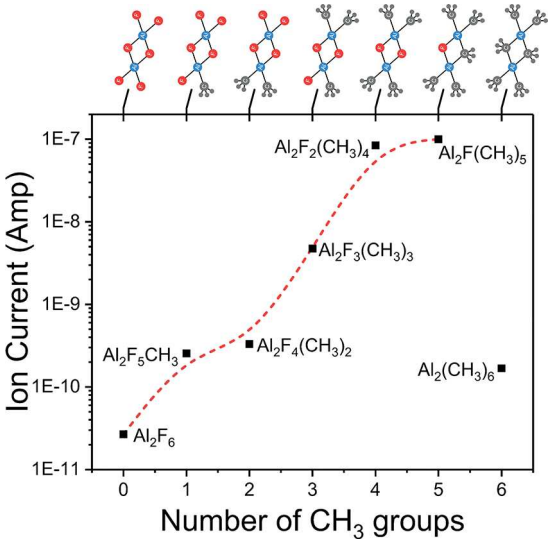

Figure 16. Ion currents for $Al_2F_x(CH_3)_y$ dimers after ligand-exchange reaction of $Al(CH_3)_3$ with HF-fluorinated Al_2O_3 powder at 300 °C plotted versus *y*, the number of CH_3 groups.

The highest ion signals are for Al_2FMe_5 (μ-methyl-μ-fluoridotetramethyldialuminum) shown in Figure 15n and $Al_2F_2Me_4$ (di-μ-fluoridotetramethyldialuminum) displayed in Figure 15g. These dimers have one or two strong Al−F−Al bridge bonds and four terminal CH_3 ligands that facilitate desorption from the AlF_3 surface. The ion currents decrease as F atoms are progressively placed in the terminal positions for $Al_2F_3Me_3$ shown in Figure 15f (di-μ-fluorido-trimethylfluorido-aluminum), $Al_2F_4Me_2$ displayed in Figures 15d and 15e (di-μ-fluorido-*cis*-dimethylfluoridoaluminuium and di-μ-fluorido-*trans*-dimethylfluoridoaluminum), and Al_2F_5Me illustrated in Figure 15b (di-μ-fluoridomethyltrifluoridodialuminum).

Based on the theoretical and QMS results, the dominant species leaving the HF-fluorinated Al_2O_3 surface during the ligand-exchange reaction with TMA are $Al_2F(CH_3)_5$ shown in Figure 15n (μ-methyl-μ-fluorido-tetramethyldialuminum) and $Al_2F_2(CH_3)_4$ displayed in Figure 15g (di-μ-fluorido-tetramethyldialuminum). Upon ionization, these dimers lose a CH_3 group and are detected as $Al_2F(CH_3)_4^+$ at m/z = 133 and $Al_2F_2(CH_3)_3^+$ at m/z = 137. The $Al_3F_3(CH_3)_5$ trimer is also expected to have three Al−F−Al bridge bonds and four terminal CH_3 ligands as shown in Figure 5. This trimer is detected as $Al_3F_3(CH_3)_5^+$ at m/z = 213.

IV. CONCLUSIONS

In situ QMS was used to characterize the volatile etch species produced during the fluorination and ligand-exchange reactions during thermal Al_2O_3 ALE. The thermal Al_2O_3 ALE was performed using HF and $Al(CH_3)_3$ (trimethyl-aluminum, TMA) at 300 °C. The QMS measurements showed that H_2O is the predominant product produced during the fluorination of Al_2O_3 powder with HF. During the ligand-exchange reaction between TMA and HF-fluorinated Al_2O_3 powder, the QMS results revealed prominent molecular ions at $Al_2F(CH_3)_4^+$ at m/z = 133 and $Al_2F_2(CH_3)_3^+$ at m/z = 137. These molecular ions are believed to result from dimers of $AlF(CH_3)_2$ (dimethylaluminum fluoride (DMAF) with itself (DMAF + DMAF) or with TMA (DMAF + TMA) after the loss of a methyl group. Another important molecular ion is a trimer detected as $Al_3F_3(CH_3)_5^+$ at m/z = 213.

Nearly equivalent results were observed for TMA exposures on AlF_3 powder. This equivalence indicates that the surface of HF-fluorinated Al_2O_3 powder and the surface of AlF_3 powder are nearly identical for the TMA ligand-exchange reaction. Thermal Al_2O_3 ALE was confirmed by TEM studies of Al_2O_3 ALD films on W powders. TEM images before and after various numbers of thermal Al_2O_3 ALE cycles using HF and TMA as the reactants revealed that the etch process was uniform and conformal.

By use of $AlCl(CH_3)_2$ (dimethylaluminum chloride, (DMAC)) as the metal precursor for ligand exchange on AlF_3 powder, the main molecular ions observed by QMS were the dimers $Al_2F(CH_3)_4^+$ at m/z = 133 and $Al_2F_2(CH_3)_3^+$ at m/z = 137 and the trimer $Al_3F_3(CH_3)_5^+$ at m/z = 213. Mixed-halogen products, such as the dimers $Al_2FCl(CH_3)_3^+$ at m/z = 153 and $Al_2F_2Cl(CH_3)_2^+$ at m/z = 157 and the trimer

DOI: 10.1021/acs.jpcc.9b06104
J. Phys. Chem. C 2020, 124, 287−299

$Al_3F_3Cl(CH_3)_4^+$ at m/z = 233, were also observed at lower signal intensities. During ligand exchange, either Cl or CH_3 ligands could transfer between DMAC and AlF_3. The similarity of the TMA and DMAC results argues that CH_3 is the dominant species during the ligand-exchange reaction for both TMA and DMAC.

$SiCl_4$ and $TiCl_4$ do not lead to thermal Al_2O_3 ALE at 300 °C. In agreement with these results, QMS measurements revealed no Al-containing etch species after $SiCl_4$ and $TiCl_4$ exposures on AlF_3 powder at 300 °C. $SiF_xCl_y^+$ and $TiF_xCl_y^+$ species were observed which indicated that ligand exchange can occur without the release of Al-containing etch species. These results suggest that $AlClF_2$ species formed after the ligand-exchange reaction are not able to desorb from the AlF_3 surface.

Quantum chemical calculations verified that dimer products are energetically more stable than monomer products. In addition, dimer products with two Al−F−Al bridging bonds are the most stable and dimers with two Al−CH_3−Al bridging bonds are the least stable. These results also suggest that dimers with terminal CH_3 ligands are most able to desorb from the surface because these dimers need to break weak Al−CH_3−Al bridging bonds. This suggestion was supported by the QMS results showing that the ion signals from the $Al_2F_2(CH_3)_4$ or $Al_2F(CH_3)_5$ dimers with 4 or 5 methyl groups are much higher than the ion signals from the $Al_2F_3(CH_3)_3$, $Al_2F_4(CH_3)_2$, or $Al_2F_5(CH_3)$ dimers with 3, 4, or 5 fluorine ligands.

AUTHOR INFORMATION

Corresponding Author

*E-mail: Steven.George@Colorado.edu.

ORCID

James E. T. Smith: 0000-0002-5130-8633
Sandeep Sharma: 0000-0002-6598-8887
Steven M. George: 0000-0003-0253-9184

Notes

The authors declare no competing financial interest.

ACKNOWLEDGMENTS

This research was funded by the Lam Research Corporation. Additional support was provided by the National Science Foundation (CHE-1609554 and CHE-1800584). The authors are also grateful to the Defense Advanced Research Projects Agency (DARPA) for seed funds to build the custom reactor with *in situ* QMS. J.E.T.S. gratefully acknowledges support from a fellowship through The Molecular Sciences Software Institute under NSF Grant ACI1547580. This work utilized the RMACC Summit supercomputer, which is supported by the National Science Foundation (ACI-1532235 and ACI-1532236), the University of Colorado Boulder, and Colorado State University. The authors thank the University of Colorado Boulder for startup funds used to pay for allocations on the Summit supercomputer.

REFERENCES

(1) Kanarik, K. J.; Lill, T.; Hudson, E. A.; Sriraman, S.; Tan, S.; Marks, J.; Vahedi, V.; Gottscho, R. A. Overview of Atomic Layer Etching in the Semiconductor Industry. *J. Vac. Sci. Technol., A* **2015**, *33*, 020802.

(2) Lee, Y.; George, S. M. Atomic Layer Etching of Al_2O_3 Using Sequential, Self-Limiting Thermal Reactions with $Sn(acac)_2$ and HF. *ACS Nano* **2015**, *9*, 2061−2070.

(3) Faraz, T.; Roozeboom, F.; Knoops, H. C. M.; Kessels, W. M. M. Atomic Layer Etching: What Can We Learn from Atomic Layer Deposition? *ECS J. Solid State Sci. Technol.* **2015**, *4*, N5023−N5032.

(4) George, S. M. Atomic Layer Deposition: An Overview. *Chem. Rev.* **2010**, *110*, 111−131.

(5) Lee, Y.; DuMont, J. W.; George, S. M. Atomic Layer Etching of AlF_3 Using Sequential, Self-Limiting Thermal Reactions with $Sn(acac)_2$ and Hydrogen Fluoride. *J. Phys. Chem. C* **2015**, *119*, 25385−25393.

(6) Johnson, N. R.; Sun, H. X.; Sharma, K.; George, S. M. Thermal Atomic Layer Etching of Crystalline Aluminum Nitride Using Sequential, Self-limiting Hydrogen Fluoride and $Sn(acac)_2$ Reactions and Enhancement by H_2 and Ar Plasmas. *J. Vac. Sci. Technol., A* **2016**, *34*, 050603.

(7) Lee, Y.; DuMont, J. W.; George, S. M. Atomic Layer Etching of HfO_2 Using Sequential, Self-Limiting Thermal Reactions with $Sn(acac)_2$ and HF. *ECS J. Solid State Sci. Technol.* **2015**, *4*, N5013−N5022.

(8) DuMont, J. W.; George, S. M. Competition Between Al_2O_3 Atomic Layer Etching and AlF_3 Atomic Layer Deposition Using Sequential Exposures of Trimethylaluminum and Hydrogen Fluoride. *J. Chem. Phys.* **2017**, *146*, 052819.

(9) Lee, Y.; Huffman, C.; George, S. M. Selectivity in Thermal Atomic Layer Etching Using Sequential, Self-Limiting Fluorination and Ligand-Exchange Reactions. *Chem. Mater.* **2016**, *28*, 7657−7665.

(10) Puurunen, R. L. Surface Chemistry of Atomic Layer Deposition: A Case Study for the Trimethylaluminum/water Process. *J. Appl. Phys.* **2005**, *97*, 121301.

(11) Lee, Y.; DuMont, J. W.; Cavanagh, A. S.; George, S. M. Atomic Layer Deposition of AlF_3 Using Trimethylaluminum and Hydrogen Fluoride. *J. Phys. Chem. C* **2015**, *119*, 14185−14194.

(12) DuMont, J. W.; Marquardt, A. E.; Cano, A. M.; George, S. M. Thermal Atomic Layer Etching of SiO_2 by a "Conversion-Etch" Mechanism Using Sequential Reactions of Trimethylaluminum and Hydrogen Fluoride. *ACS Appl. Mater. Interfaces* **2017**, *9*, 10296−10307.

(13) Zywotko, D. R.; George, S. M. Thermal Atomic Layer Etching of ZnO by a "Conversion-Etch" Mechanism Using Sequential Exposures of Hydrogen Fluoride and Trimethylaluminum. *Chem. Mater.* **2017**, *29*, 1183−1191.

(14) Johnson, N. R.; George, S. M. WO_3 and W Thermal Atomic Layer Etching Using "Conversion-Fluorination" and "Oxidation-Conversion-Fluorination" Mechanisms. *ACS Appl. Mater. Interfaces* **2017**, *9*, 34435−34447.

(15) Lee, Y.; George, S. M. Thermal Atomic Layer Etching of Titanium Nitride Using Sequential, Self-Limiting Reactions: Oxidation to TiO_2 and Fluorination to Volatile TiF_4. *Chem. Mater.* **2017**, *29*, 8202−8210.

(16) Abdulagatov, A. I.; George, S. M. Thermal Atomic Layer Etching of Silicon Using O_2, HF, and $Al(CH_3)_3$ as the Reactants. *Chem. Mater.* **2018**, *30*, 8465−8475.

(17) Gertsch, J. C.; Cano, A. M.; Bright, V. M.; George, S. M. SF_4 as the Fluorination Reactant for Al_2O_3 and VO_2 Thermal Atomic Layer Etching. *Chem. Mater.* **2019**, *31*, 3624−3635.

(18) Johnson, N. R.; Hite, J. K.; Mastro, M. A.; Eddy, C. R.; George, S. M. Thermal Atomic Layer Etching of Crystalline GaN Using Sequential Exposures of XeF_2 and BCl_3. *Appl. Phys. Lett.* **2019**, *114*, 243103.

(19) Lee, Y.; George, S. M. Thermal Atomic Layer Etching of HfO_2 Using HF for Fluorination and $TiCl_4$ for Ligand-Exchange. *J. Vac. Sci. Technol., A* **2018**, *36*, 061504.

(20) Olah, G. A.; Nojima, M.; Kerekes, I. Synthetic Methods and Reactions 0.2. Hydrofluorination of Alkenes, Cyclopropane and Alkynes with (Trialkylamine) Reagents. *Synthesis* **1973**, *1973*, 779−780.

DOI: 10.1021/acs.jpcc.9b06104
J. Phys. Chem. C 2020, 124, 287−299

(21) Lin, T.; Kang, B.; Jeon, M.; Huffman, C.; Jeon, J.; Lee, S.; Han, W.; Lee, J.; Lee, S.; Yeom, G.; et al. Controlled Layer-by-Layer Etching of MoS_2. *ACS Appl. Mater. Interfaces* **2015**, *7*, 15892−15897.
(22) Frisch, M. J.; Trucks, G. W.; Schlegel, H. B.; Scuseria, G. E.; Robb, M. A.; Cheeseman, J. R.; Scalmani, G.; Barone, V.; Petersson, G. A.; Nakatsuji, H.; et al. *Gaussian 16*, Rev. B.01; Gaussian Inc.: Wallingford, CT, 2016.
(23) Yu, H. S.; He, X.; Truhlar, D. G. MN15-L: A New Local Exchange-Correlation Functional for Kohn-Sham Density Functional Theory with Broad Accuracy for Atoms, Molecules, and Solids. *J. Chem. Theory Comput.* **2016**, *12*, 1280−1293.
(24) Binkley, J. S.; Pople, J. A.; Hehre, W. J. Self-Consistent Molecular Orbital Methods. 21. Small Split-Valence Basis Sets for 1st Row Elements. *J. Am. Chem. Soc.* **1980**, *102*, 939−947.
(25) Gordon, M. S.; Binkley, J. S.; Pople, J. A.; Pietro, W. J.; Hehre, W. J. Self-Consistent Molecular Orbital Methods. 22. Small Split-Valence Basis Sets for 2nd Row Elements. *J. Am. Chem. Soc.* **1982**, *104*, 2797−2803.
(26) Cizek, J. In *Advances in Chemical Physics*; Hariharan, P. C., Ed.; Wiley Interscience: New York, 1969; Vol. *14*, p 35.
(27) Purvis, G. D.; Bartlett, R. J. A Full Coupled-Cluster Singles and Doubles Model - The Inclusion of Diconnected Triples. *J. Chem. Phys.* **1982**, *76*, 1910−1918.
(28) Scuseria, G. E.; Janssen, C. L.; Schaefer, H. F. An Efficient Reformulation of the Closed-Shell Coupled Cluster Single and Double Excitation (CCSD) Equations. *J. Chem. Phys.* **1988**, *89*, 7382−7387.
(29) Scuseria, G. E.; Schaefer, H. F. Is Coupled Cluster Singles and Doubles (CCSD) More Computationally Intensive Than Quadratic Configuration-Interactions (QCISD). *J. Chem. Phys.* **1989**, *90*, 3700−3703.
(30) Dill, K. A.; Bromberg, S. *Molecular Driving Forces: Statistical Thermodynamics in Biology, Chemistry, Physics and Nanoscience*; Garland Science: 2011.
(31) Kanchanakungwankul, S.; Bao, J. L.; Zheng, J.; Alecu, I. M.; Bynch, B. J.; Zhao, Y.; Trular, D. G. Database of Frequency Scale Factors for Electronic Model Chemistries (2017). Retrieved from https://comp.chem.umn.edu/freqscale/190107_Database_of_Freq_Scale_Factors_v4.pdf.
(32) Anderson, J.; Burns, P. J.; Milroy, D.; Ruprecht, P.; Hauser, T.; Siegel, H. J. Deploying RMACC Summit: An HPC Resource for the Rocky Mountain Region, *Proceedings of PEARC17*, New Orleans, LA, July 9−13, 2017; p 7.
(33) Natarajan, S. K.; Elliott, S. D. Modeling the Chemical Mechanism of the Thermal Atomic Layer Etch of Aluminum Oxide: A Density Functional Theory Study of Reactions during HF Exposure. *Chem. Mater.* **2018**, *30*, 5912−5922.
(34) Weidlein, J.; Krieg, V. Vibrational Spectra of Dimethyl and Diethyl Aluminum Fluoride. *J. Organomet. Chem.* **1968**, *11*, 9−16.
(35) Carlsson, J. O.; Gorbatkin, S.; Lubben, D.; Greene, J. E. Thermodynamics of the Homogeneous and Heterogeneous Decompostion of Trimethylaluminum, Monomethylaluminum, and Dimethylaluminumhydride - Effects of Scavengers and Ultraviolet Laser Photolysis. *J. Vac. Sci. Technol., B: Microelectron. Process. Phenom.* **1991**, *9*, 2759−2770.
(36) Laubengayer, A. W.; Gilliam, W. F. The Alkyls of the Third Group Elements. I. Vapor Phase Studies of the Alkyls of Aluminum, Gallium and Indium. *J. Am. Chem. Soc.* **1941**, *63*, 477−479.
(37) Almenningen, A.; Halvorsen, S.; Haaland, A. Molecular Structure of the Trimethylaluminum Monomer. *J. Chem. Soc. D* **1969**, 644.
(38) Brockway, L. O.; Davidson, N. R. The Molecular Structure of the Dimers of Aluminum Dimethyl Chloride, Aluminum Dimethyl Bromide, and Aluminum Trimethyl and of Hexamethyldisilane. *J. Am. Chem. Soc.* **1941**, *63*, 3287.
(39) Davidson, N.; Brown, H. C. The Polymerization of Some Derivatives of Trimethylaluminum. *J. Am. Chem. Soc.* **1942**, *64*, 316−324.
(40) Fowler, R. M.; Melford, S. S. $FeAlCl_6$, A Volatile Molecule Formed by the Reaction of Aluminum Chloride with Ferric Chloride. *Inorg. Chem.* **1976**, *15*, 473−474.
(41) Varga, Z.; Kolonits, M.; Hargittai, M. Comprehensive Study of the Structure of Aluminum Trihalides from Electron Diffraction and Computation. *Struct. Chem.* **2012**, *23*, 879−893.
(42) Dewing, E. W. Gaseous Complexes Formed Between Trichlorides ($AlCl_3$ and $FeCl_3$) and Dichlorides. *Metall. Trans. A* **1970**, *1*, 2169−2174.
(43) Papatheodorou, G. N. Spectrophotometric Study of Platinum-(II) Chloride-Aluminum Chloride Vapor Complex. *Inorg. Chem.* **1973**, *12*, 1899−1902.
(44) Binnewies, M.; Glaum, R.; Schmidt, M.; Schmidt, P. *Chemical Vapor Transport Reactions*; Walter de Gruyter GmbH & Co.: Berlin, 2012.
(45) Schafer, H. Gaseous Chloride Complexes with Halogen Bridges- Homo-Complexes and Hetero-Complexes. *Angew. Chem., Int. Ed. Engl.* **1976**, *15*, 713−727.
(46) Schafer, H. Gaseous Chloride Complexes Containing Halogen Bridges. *Adv. Inorg. Chem.* **1983**, *26*, 201−234.
(47) Porter, R. F.; Zeller, E. E. Mass Spectra of Aluminum(III) Halides and the Heats of Dissociation of $Al_2F_6(g)$ and $LiF\text{-}AlF_3(g)$. *J. Chem. Phys.* **1960**, *33*, 858−863.
(48) Gundersen, G.; Haugen, T.; Haaland, A. On the Molecular Structure of Dimethylaluminum Fluoride Tetramer, $[(CH_3)_2AlF]_4$. *J. Organomet. Chem.* **1973**, *54*, 77−86.
(49) Cano, A. M.; Marquardt, A. E.; DuMont, J. W.; George, S. M. Effect of HF Pressure on Thermal Al_2O_3 Atomic Layer Etch Rates and Al_2O_3 Fluorination. *J. Phys. Chem. C* **2019**, *123*, 10346−10355.
(50) *HSC Chemistry*; HSC Chemistry 5.1; Outokumpu Research Oy: Pori, Finland.
(51) Roesky, H. W.; Haiduc, I. Fluorine as a Structure-Directing Element in Organometallic Fluorides: Discrete Molecules, Supramolecular Self-Assembly and Host-Guest Complexation. *J. Chem. Soc., Dalton Trans.* **1999**, 2249−2264.

DOI: 10.1021/acs.jpcc.9b06104
J. Phys. Chem. C 2020, 124, 287−299